Spectroscopy and Photoinduced Dynamics of ICN and Its Photoproducts in Solid Argon†

J. Helbing and M. Chergui*

Institut de Physique de la Matière Condensée, BSP, Université de Lausanne, CH-1015 Lausanne-Dorigny, Switzerland

Received: April 3, 2000; In Final Form: June 12, 2000

The photochemistry of ICN isolated in Ar matrixes has been investigated using UV absorption and laser spectroscopy under a variety of experimental conditions. Laser excitation of the repulsive Ã continuum gives rise to long-lived near-infrared emission from stabilized I and CN fragments in the shallow excited $^3\Pi_2$ potential and to the formation of the INC isomer. The latter is identified by its UV absorption band, which overlaps the ICN UV absorption. A photoinduced equilibrium is rapidly established between the two species under 250-nm irradiation, in line with the interpretation of previously published IR data (Samuni, U. et al. *Chem. Phys. Lett.* **1994**, *225*, 391). This equilibrium can be shifted in favor of either species by the choice of irradiation wavelength. Permanent dissociation and the stabilization of CN fragments under UV irradiation is also reported, but the dissociation efficiency depends strongly on experimental conditions. This observation allows for the reconciliation of conflicting views in the literature on the photostability of ICN in solid argon.

I. Introduction

Even the simplest photochemical reaction, e.g., unimolecular dissociation, becomes a complex problem in the condensed phase. The presence of a solvent cage alters the outcome of the reaction in several ways: (a) it may hinder the permanent separation of fragments or significantly reduce its probability, (b) caged fragments may recombine in the ground or bound excited states, (c) the cage may even stabilize fragments on otherwise purely repulsive excited-state surfaces because of the steric hindrance it exerts on the separation of the dissociation products, and (d) the solvent may alter the energetics and the coupling between potential energy surfaces.[1,2]

In liquids, the medium fluctuations make it difficult to pinpoint the details of the different physical processes occurring during such a reaction, but in the case of simple diatomics, the development of femtosecond spectroscopy now allows one to circumvent such difficulties by an appropriate separation of time scales.[3]

Another approach has been to use cryogenic matrixes, which provide a rigid cage and in which the different processes can, in principle, be studied separately. This has mainly been the work of groups in Berlin and Irvine, who carried out systematic studies of the cage effect on the dissociation of small molecules such as H_2O, H_2S, HCl, and halogens.[1,2,4−10]

In diatomic molecules such as I_2, the combination of femtosecond spectroscopy and the matrix isolation technique has allowed a very detailed description of the dynamics following dissociation, in part with the help of molecular dynamics simulations.[9−11] In triatomic molecules such as H_2O or H_2S, it is the atomic H fragment that carries most of the kinetic energy. Therefore, the ensuing dynamics are similar to those occurring in diatomics, i.e., there is only one significant intramolecular reaction coordinate. A further degree of complication occurs when the lighter fragment is a diatom and when it carries internal energy in the form of rotation or vibration. In such a case, one anticipates more complex dynamics, which may lead to interesting effects such as cage-induced isomerization.

In undertaking this work, our primary interest was to probe, in real time, the dynamics of ICN dissociation in Ar matrixes. However, a prerequisite for such a study is the identification of spectroscopic observables to be used to probe the dynamics. The spectroscopy of ICN and its photoproducts alone already reveals an interesting photoinduced chemistry of ICN-doped solid Ar, which will be presented in this contribution. The choice of ICN is motivated by several reasons, as follows.

The UV photodissociation of ICN has long been used for benchmark gas-phase experiments, allowing a detailed comparison between theory and experiment.[12−25] The particular interest in this molecule stems from the fact that excitation of the purely dissociative Ã-band system between 200 and 300 nm yields iodine atoms in both their ground and spin-excited states, with very different vibrational and rotational distributions for the corresponding CN fragments.[19−21] Ab initio potential surface calculation by Morokuma et al.[12,13] stimulated extensive theoretical studies,[13−16] which yielded results in good agreement with experiment. It is now commonly believed that nonadiabatic coupling between three electronic states ($^1\Pi_1$, $^3\Pi_{0^+}$, and $^3\Pi_1$) largely determines the vibrational and rotational energy distributions of the CN fragment. Femtosecond pump−probe experiments have also provided a wealth of details about the photodissociation dynamics.[24,25]

A condensed-phase environment is expected to alter both the dissociative character of the excited-state surfaces of ICN (caging) and their coupling, making ICN under UV excitation an ideal model system for studying the influence of solvation on reaction dynamics.[26]

Classical trajectory calculations in liquid environments have generally predicted a high probability for cage exit of the CN fragment.[27−29] On the other hand, in the case of solids, a very efficient recombination of ICN and isomerization (I−CN → I−NC) on the excited-state surfaces have been predicted.[29,30] Comparisons with experiments in the condensed phase are,

† Part of the special issue "C. Bradley Moore Festschrift".

* Author to whom correspondence should be addressed.

10.1021/jp0012754 CCC: $19.00
Published on Web 08/15/2000

however, much more difficult. In the liquid solvents studied so far,[31,32] chemical reactions of the fragments with the solvent species play a role that further complicates the dynamics, while in the nonreactive (solid) environments such as rare gas matrixes, and especially solid Ar, conflicting conclusions were drawn in studies using different experimental techniques.

Already back in 1969, Easley and Weltner[33] identified CN fragments by ESR spectroscopy following UV photolysis of ICN in Ne, Ar, and Kr matrixes with a Hg lamp. However, they could not observe the CN absorption at 2044 cm^{-1} in the infrared region. Instead, a band at 2057 cm^{-1} was found. This band was also seen by Carr et al.[34] using the same irradiation source, and it was assigned to the INC isomer. Leutwyler et al.[35] found evidence of CN radical formation after VUV irradiation of ClCN and BrCN but found that ICN is stable. Heaven et al.[36] observed CN fragments in large Ar_n clusters doped with ICN as a precursor, but it is not clear whether the CN fragments were formed during or after cluster formation. In a series of IR absorption experiments, Haas and co-workers[37,38] found no evidence for ICN UV dissociation in Ar, Kr, and Xe matrixes but reported new bands in the 400−2060 cm^{-1} region, which they attributed to the INC isomer. This attribution was supported by quantum-chemical calculations and isotope-substitution experiments,[38] and the absence of cage exit for the CN fragment was confirmed by MD simulations.[29] Much earlier, Milligan and Jacox[39] reported new absorption bands in the CN stretch region following vacuum ultraviolet photolysis of XCN (X = H, F, Cl, Br) molecules trapped in cryogenic matrixes, which they attributed tentatively to XNC species. The observation of INC isomers by Haas et al.[37,38] would be in line with these results.

In this work, we have carried out an extensive study of ICN isolated in Ar matrixes using the very sensitive technique of UV−vis optical spectroscopy. We will present results of spectroscopy and photoinduced dynamics of ICN in solid argon that provide new information on fragment caging and the ICN−INC isomerization process in argon and confirm the presence of permanent dissociation. By comparing data obtained under different sample preparation conditions, we are able to show that the contradictions between previous results can be explained by considering the specific experimental conditions.

II. Experiment

Commercially available ICN (purity 95−97%, Aldrich) was used both with and without further purification by sublimation (yielding a snow-white color). However, we found that the purity of the solid had no influence on the results. ICN vapor at room temperature (ca. 1 mbar) was premixed with Ar (6.0) at ratios ranging from 1:300 to 1:2000, and the gas mixture was condensed onto an MgF_2 or LiF window cooled to temperatures between 4 and 40 K by a cryostat in a UHV chamber (background pressure < 10^{-9} mbar). The sample growth was controlled by monitoring the interference pattern produced by a He−Ne laser reflected off the sample. Very high optical quality ICN/Ar samples were obtained with growth rates of approximately 10 μm h^{-1} at 20 K, typically over the course of 3−6 h. When grown at a temperature of 4 K, the samples were of poor crystalline quality and showed very different photochemical behavior.

Given the weak oscillator strength of ICN for absorption in the UV,[40,41] we also devised a new type of sample holder, to ensure that photoinduced changes in the UV spectroscopy of the samples are not due to the substrate. This sample holder consists of a free-standing 2-mm-thick pure Ar crystal onto which ICN-doped Ar films are deposited. This sample preparation technique should be particularly attractive for studies in the UV and VUV domains, where prolonged irradiation is known to induce defects in the usually VUV-transparent substrate materials (MgF_2, LiF, CaF_2, quartz). Rare gas materials could replace these substrates, as they also have a large transparency range, extending up to 12 eV in the case of solid Ar.

In a first series of measurements, the UV transmission of the sample was monitored as a function of laser irradiation, using a stabilized deuterium lamp. Care was taken that the irradiated spot on the sample always be larger than the area probed in absorption at a 90° angle. The photon flux was determined from the measured laser power and the cross section of the beam, measured with the help of photosensitive paper or a pinhole. Different laser sources were used for irradiation, including (a) a YAG-laser-pumped optical parametric oscillator (MOPO, Spectra Physics) delivering pulses (<5 ns, 10-Hz repetition rate) that are tunable between 450 and 1500 nm, and down to 225 nm after frequency doubling; (b) an excimer Laser (Lambda Physik) that was operated at 248 nm (KrF) or at 193 nm (ArF); and (c) an amplified, frequency-tripled femtosecond laser system, generating 260-nm pulses of 200-fs duration at a repetition rate of 1 kHz.

Using the same light sources, fluorescence and fluorescence-excitation spectra were recorded for UV (ICN) and visible (CN fragment) excitation.

Transmitted light from the D_2 lamp and fluorescence light was dispersed in a monochromator and detected using a UV-enhanced (λ > 190 nm) CCD camera. For time-resolved fluorescence measurements, a photomultiplier was used in connection with a 600-MHz digital oscilloscope or a photon-counting system.

III. Results

The presentation of the results is divided in two parts. The first concerns the UV absorption spectroscopy before and after UV irradiation of the samples. The second deals with emission spectra recorded upon UV excitation.

Figure 1a shows a potential curve diagram of ICN adapted from ab initio calculations.[12,13] In the gas phase, the absorption spectrum of ICN consists of a broad band (the so-called $\tilde{A}$ band) extending from ~310 to ~210 nm and centered at ~250 nm.[41] Its oscillator strength is very low (ϵ = 100 L mol^{-1} cm^{-1} at the band maximum),[40,41] and according to the ab initio calculations,[13] it is due to absorption by the $^3\Pi_1$, $^3\Pi_{0^+}$, and $^1\Pi_1$ states. For λ < 210 nm, the so-called α band rises abruptly and contains discrete structures. It is substantially more intense than the $\tilde{A}$ band.[40] The continuum part has been attributed to transitions to dissociative $^{1,3}\Delta$, Σ^+, and Σ^- states, while the discrete structure is believed to be due to transitions to the $^1\Sigma^+$ state, which is an ionic state correlating to the $I^+(^1\Sigma) + CN^-(^1\Sigma^+)$ dissociation limit.[40]

A. Absorption Studies. Figure 2a shows the absorption spectrum of a ~40-μm-thick, ICN-doped Ar matrix grown at 20 K, with an ICN:Ar mixing ratio before deposition of ~1:300. The oscillatory structure at longer wavelengths changes rapidly during sample growth and is caused by interferences due to a thin layer of argon deposited at the back of the sample holder. The broad absorption feature at wavelengths smaller than 300 nm closely resembles the $\tilde{A}$ band of ICN in the gas-phase,[40,41] with the maximum blue shifted by ~150 meV, located at 242 ± 3 nm. Just as in the gas phase, there is also an increased absorption at λ < 210 nm, which is due to the so-

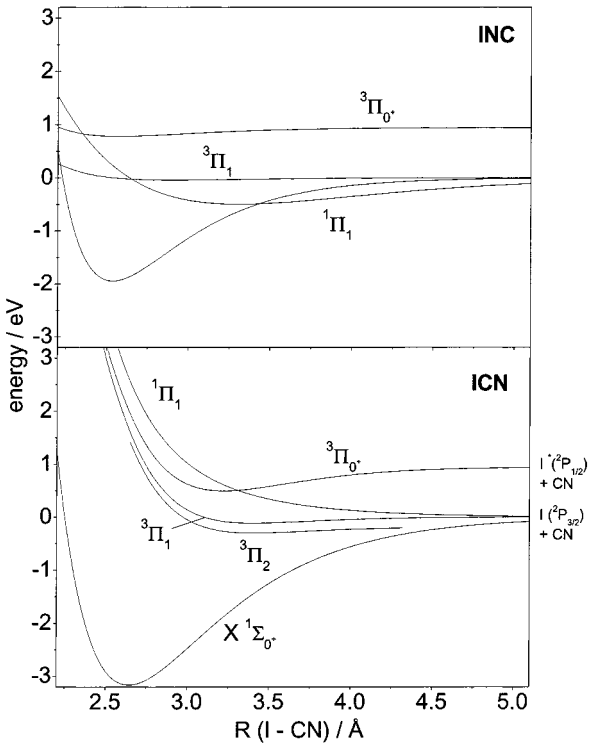

Figure 1. Potential energy curves of linear ICN and INC according to refs 12 and 13. The *R* coordinate is the distance between the center of mass of the CN molecule and the I atom.

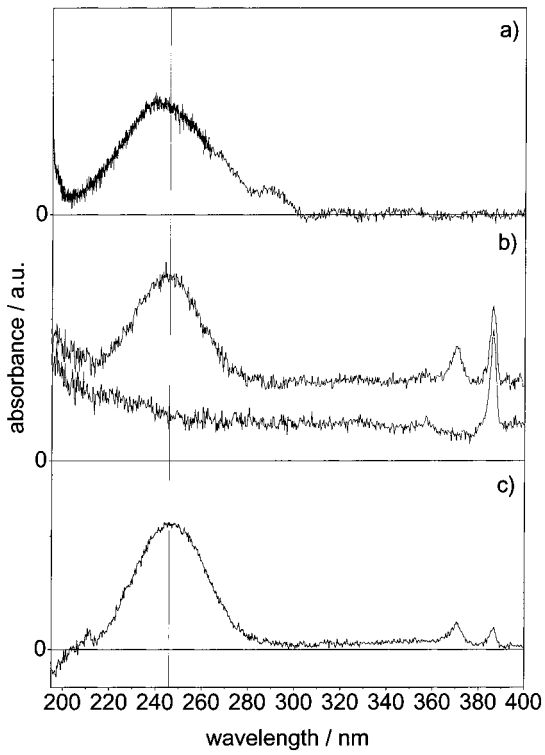

Figure 2. (a) Absorption spectrum of ICN in solid Ar (concentration $c \approx 1{:}300$). The spectrum was taken immediately after growth at 20 K. (The structure in the long-wavelength tail is caused by interferences due to a thin layer of condensate growing on the back of the sample holder.) (b) Upper trace: increase in absorption induced by an irradiation dose of $\sim 5 \times 10^{18}$ photons cm^{-1} at 248 nm and at 12 K (a spectrum taken before irradiation at 12 K served as reference). Lower trace: absorption change after irradiation at 248 nm followed by irradiation at 370 nm and 12 K. The changes induced in the 250-nm region by the 248-nm photons are completely reversed ($c \approx 1{:}500$). (c) Change in absorption induced by an irradiation dose of $\sim 2 \times 10^{20}$ photons cm^{-2} at 193 nm at 12 K. Concentration as in panel b, but saturated absorption at 245 nm is ~5 times stronger.

called α band.[40] Unfortunately, O_2 absorption and the resulting cutoff wavelength of our detection system at ~195 nm do not permit a more detailed investigation of this structure with the present setup.

An estimate of the ICN Ã-band extinction coefficient in Ar from Figure 2a yields $\epsilon = 30$ L mol^{-1} cm^{-1} at the band maximum. However, the effects of scattering, as well as the uncertainty about the deposited ICN concentration compared to that of the original gas mixture, make it difficult to determine the absolute absorption cross section with precision, and our result may well compare with the reported gas-phase value of 80−100 L mol^{-1} cm^{-1}.[41]

1. Photolysis at 250 nm. Upon irradiation of the samples at wavelengths near 250 nm, changes in sample absorption are induced even with a small irradiation dose, and at 248 nm, a steady state is reached after exposure to $\sim 2 \times 10^{18}$ photons cm^{-2}. The upper trace in Figure 2b shows the difference in absorption due to this irradiation dose, with respect to an unirradiated sample. A new, narrow absorption band appears at 370 nm, and a broad absorption increase is observed around the irradiation wavelength. The additional feature at 386 nm will be discussed below. The new broad band has its maximum at 245 ± 3 nm, and it extends to 280 nm. It differs from the original ICN absorption band in that its bandwidth is somewhat smaller and it is centered slightly further to the red. The 370- and 245-nm absorption bands are stable upon annealing to 35 K, but irradiation at the 370-nm band completely reverses the changes caused by the initial 248-nm irradiation. This can be seen in the lower trace of Figure 2b, which shows the change in absorption of a sample exposed first to 248-nm (yielding the upper trace spectrum) and then to 370-nm light. The overall result is only an increase in scattering, with the exception of the 386-nm band, which persists. Subsequent re-irradiation at 248 nm reproduces the difference spectrum shown in the upper trace, and this cycle can be repeated many times. The narrow 370-nm structure always reappears at its previous intensity, but changes in absorption between 200 and 300 nm are reduced after a few cycles, which points to a different origin for the irradiation-induced 370- and 245-nm bands. The cycle is maintained for a longer time, however, when 250- and 386-nm light is used in the cycles.

The growth of the additional absorption band at 386 nm is accompanied by a much smaller feature at 357 nm. These bands are easily identified as the $B^2\Sigma^+ \leftarrow X^2\Sigma^+$ ($v' = 0$) and ($v' = 1$) absorption bands of the CN radical,[43] formed by dissociation of ICN molecules. The growth of the CN bands occurs on a much longer time scale than that of the 370- and 245-nm bands. They remain unchanged under subsequent irradiation around 370 nm (Figure 2b) but diminish strongly (by a factor of ~2) when excited at 386 nm. In fact, it appears that excitation of CN at 386 nm leads to partial recombination of I and CN, trapped in special sites (see below). This also explains the difference between the 250-nm/370-nm and the 250-nm/386-nm irradiation cycles: in the first case, the ICN and INC concentrations diminish much more rapidly through dissociation than in the second case.

The irradiation-induced changes in absorption have been monitored systematically as a function of irradiation dose for different laser intensities and sample concentrations. The dots in Figure 3a show the strength of the CN $B^2\Sigma^+ \leftarrow X^2\Sigma^+$ (0,0) absorption maximum under irradiation at 248 nm and 12 K.

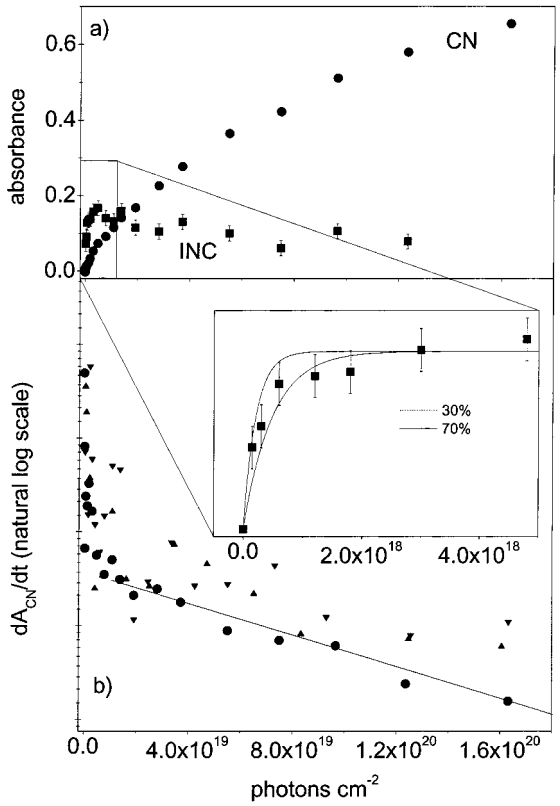

Figure 3. (a) Growth of the CN absorption band at 386 nm (●) and the INC absorption band at 245 nm (■) as a function of irradiation at 248 nm (initial ICN concentration of 1:300). The dotted and solid lines in the enlarged view of the INC growth kinetics have been calculated under the assumption of a 2.6% conversion of ICN into INC and isomerization probabilities of 30% and 70%, respectively. Data were recorded at 12 K, and the sample prepared at 20 K. (b) Slope of the CN absorption growth for samples of different initial ICN concentrations. [c = 1:300 (●), 1:1500 (▲), 1:2000 (▼)]. The data have been rescaled accordingly by multiplication by 1/c. Experimental conditions as in panel a.

The intensity changes of the 245-nm absorption band are depicted as solid squares, and an enlarged view of the early kinetics at 245 nm can be seen in the inset. Absorption at this wavelength rapidly reaches a maximum after an irradiation dose of $\sim 2 \times 10^{18}$ photons cm^{-2} and gradually loses in strength afterward. The irradiation dose necessary to reach saturation is independent of sample concentration, and the strength of the 245-nm band scales with the ICN:Ar mixing ratio before sample deposition. The same linear scaling with concentration is found for the CN absorption band. The CN growth is reminiscent of a monoexponential growth of the form

$$A_{CN}(t) = A_{CN}(\infty)(1 - e^{-\beta t}) \quad (1)$$

where $A_{CN}(t)$ is the CN absorbance. However, closer inspection of the data reveals that a fit of this form underestimates the rate of fragment formation at early times. This is illustrated in Figure 3b, where $\ln(dA_{CN}/dt)$ is plotted as a function of irradiation. This plot would yield a straight line with slope β in the case of strictly monoexponential kinetics. Instead, a "fast" and a "slow" component can be seen. The fast growth saturates very quickly at about the time when the broad band at 245 nm reaches its maximum strength, while the majority of CN fragments form during the remaining slow growth process. It can further be seen from Figure 3b that samples prepared with different ICN:Ar premixing ratios show the same kinetics of CN formation.

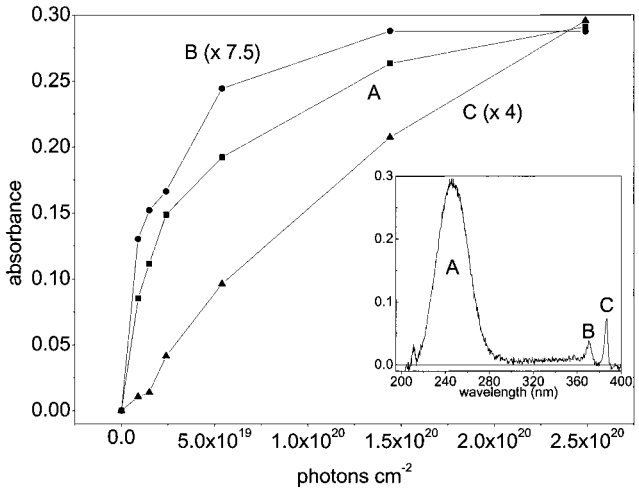

Figure 4. Growth of the absorption bands at 245 nm (■), 370 nm (●), and 386 nm (▲) as a function of irradiation at 193 nm. For better comparison, the data have been rescaled as indicated. Sample deposition at 20 K, data recorded at 12 K, $c \approx$ 1:500.

A linear fit of the dominant slow component in Figure 3b yields $\beta = (4 \pm 1) \times 10^{-21}$ cm^2, from which a dissociation probability of 3% can be calculated, making use of the gas-phase absorption cross section of ICN ($\sigma = 1.66 \times 10^{-19}$ cm^2, $\epsilon = 100$ L mol^{-1} cm^{-1} [41]). This value is, however, uncertain to within a factor of 2−3, mainly because of the difficult estimate of the photon flux. In addition, unlike the quickly saturating, irradiation-induced bands at 245 and 370 nm, the CN absorption bands are strongly reduced by annealing (similar to the reduction occurring upon irradiation of the band itself at 386 nm). In fact, the observed growth rate of the CN bands is strongly temperature dependent and is much slower when the sample is held at 20 K instead of 12 K or below during irradiation. This suggests that an equilibrium sets in between permanent dissociation and thermally induced recombination at higher temperatures, as confirmed by fluorescence measurements, which are discussed below. Because of these complications, a more precise value for the "permanent" dissociation efficiency of ICN cannot be provided.

2. Photolysis at 193 nm. Changes in sample absorption are even more drastic upon 193-nm irradiation (Figure 2c). The same new absorption bands at 370 and 245 nm are observed as after 250-nm irradiation. The feature at 370 nm grows to a strength similar to that of the corresponding band under 250-nm irradiation, but the broad 245-nm band now continues to grow much stronger and saturates only after a much larger irradiation dose. Its growth is accompanied by an increase in transmission for wavelengths smaller than 200 nm. Probably because of the much better statistics in this case, one can now also discern a narrow absorption peak at 210 nm forming alongside the broad structure at 245 nm. A very broad, weak absorption band, which extends from 280 to 400 nm, also seems to be forming, but this new feature is less certain as scattering increases with irradiation of the sample, making the contours of this broad band difficult to distinguish. CN absorption at 386 and 357 nm equally grows upon 193-nm irradiation and again on a much longer time scale than the 245-nm band.

The kinetics of these various bands as a function of irradiation dose are plotted in Figure 4. The growth curves of the 370- and 386-nm bands have been rescaled to allow a better comparison. Clearly, the three bands grow on different time scales. The 370-nm band saturates first, while the 245-nm band reaches a 5−10 times larger strength than it did under 248-nm irradiation

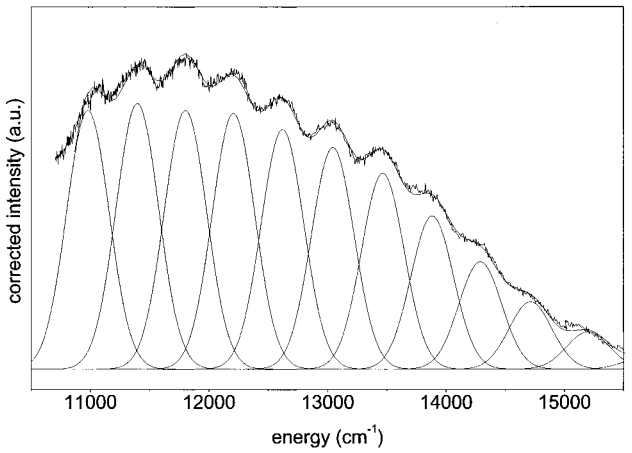

Figure 5. IR emission observed under 250-nm excitation of ICN in solid Ar. The data have been corrected for the detection efficiency of the CCD camera and fit by Gaussian line shapes of fixed width (fwhm = 420 cm^{-1}). Sample deposition at 20 K, data recorded at 12 K, $c \approx$ 1:1000.

(the absorbance of the ICN band maximum in this sample had been 0.08 before irradiation). The increase in transmission (bleach) below 200 nm appears to be correlated with the growth of the 245-nm absorption band, but stronger scattering at these wavelengths prevents us from being more affirmative.

Just as in the case of samples irradiated at 250 nm, the new absorption bands formed under 193-nm irradiation disappear again when the sample is subsequently subjected to laser light in the 370−400-nm region (the CN bands are only reduced for irradiation at 386 nm but are otherwise unaffected). During this reverse process, the kinetics of the band at 370 nm are again more rapid than those of the broad band at 245 nm. Annealing at 35 K has no effect on the broad band at 245 nm, but the already "saturated" 370-nm band grows again upon further irradiation at 193 nm after annealing. Finally, the 245-nm band, formed under previous 193-nm irradiation, is strongly reduced upon subsequent irradiation at 250 nm, while the 370-nm band is less affected. This change is reversed completely by subsequent re-irradiation at 193 nm, and this cycle can be repeated many times.

B. Fluorescence. *1. Spectroscopy.* Upon excitation of the samples at wavelengths between 220 and 310 nm, we observe a broad, weakly structured fluorescence in the near-infrared (Figure 5). The maximum of this emission lies at ∼12 000 cm^{-1}. A fit of the data with Gaussian line shapes of fwhm = 420 cm^{-1} yields an average spacing of the peak maxima of 415 cm^{-1} and no significant anharmonicity. At higher temperatures (30 K), the emission intensity decreases, and the structure is washed out, but this change is reversed when the sample is cooled back to 4 K, thereby suggesting phonon-induced broadening and nonradiative relaxation processes. The fluorescence shows a monoexponential decay with a time constant of 320 ± 20 μs, identical at all wavelengths and independent of the history of the sample (annealing, irradiation). A linear dependence of fluorescence and laser intensity was found, which excludes a multiphoton process as the cause of this emission. For 250-nm excitation, a previous irradiation of the sample at 193 nm leads to a strong increase in intensity of the broad 800-nm emission, immediately after the 250-nm laser light is turned on. It quickly becomes weaker with 250-nm irradiation, but the fluorescence can again be enhanced strongly by short 193-nm irradiation. This cycle occurs in parallel to the changes observed in absorption for alternating 193- and 250-nm irradiation. The IR

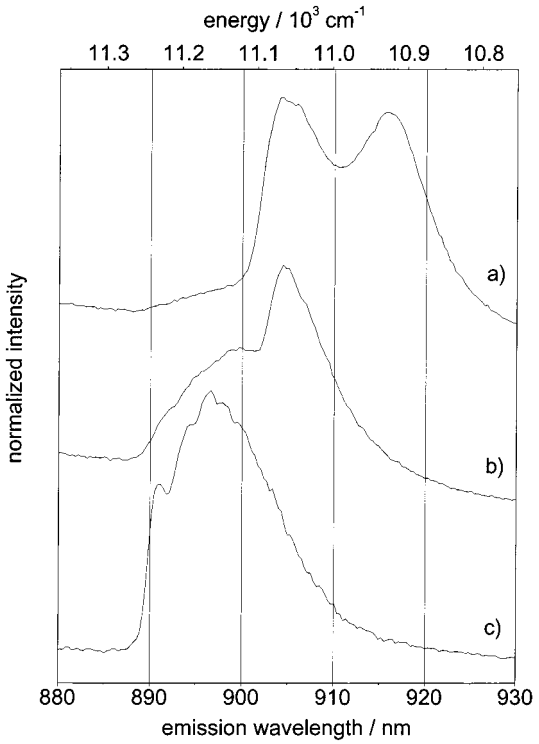

Figure 6. CN emission bands forming upon UV irradiation of ICN-doped solid Ar, recorded at 4K upon excitation at the same wavelength (250 nm). (a) Sample grown at 4 K, before annealing; (b) sample grown at 20 K, before annealing; and (c) spectrum observed after annealing of the irradiated sample (grown at 20 K). All spectra were recorded at 4 K, ICN concentration ≈ 1:1000. The ICN emission band shown in Figure 5 is underlying the spectra and is responsible for the increasing background toward shorther wavelengths.

fluorescence is equally observable under 193-nm excitation, but superimposed are two much more intense and narrower emission bands at 380 and 570 nm (with lifetimes of 15 ns). We have observed similar bands upon VUV excitation of ICN isolated in Ne and Kr matrixes, and their strong matrix shifts suggest emission from a higher-lying charge-transfer state of ICN. A detailed discussion of the VUV spectroscopy of matrix-isolated ICN will be the subject of a forthcoming publication.[42] Here, we concentrate on the photoinduced dynamics upon UV excitation.

After prolonged exposure to laser light around 250 nm (or 193 nm), additional narrow emission bands can be seen in the 900-nm region (Figure 6). The relative strength of these bands strongly depends on temperature and sample preparation conditions. With samples slowly grown at 20 K and irradiated at 4 K, a band at 905 nm (with a narrow peak at 903 nm under higher resolution) appears slowly (Figure 6b). For a sample prepared and irradiated at 4 K (strongly scattering), an additional emission band at 915 nm forms (Figure 6a), which quickly saturates. Upon annealing of the sample, both bands transform into an emission structure with a zero-phonon line at 890 nm and a broad phonon band centered at 896 nm (Figure 6c), identical to that observed for the $A^2\Pi \rightarrow X^2\Sigma^+$ (1,0) transition of isolated CN radicals in Ar matrixes.[43] Under irradiation at 12 K, the 896-nm band is dominant even before annealing. In this case, annealing only leads to a narrowing of the band and an accentuation of the zero-phonon line. It is important to note that the growth of these bands is more than an order of magnitude faster in samples prepared at 4 K than in samples prepared at 20 K. It is always accompanied by a similar decrease in strength of the broad IR emission around 800 nm. Excitation

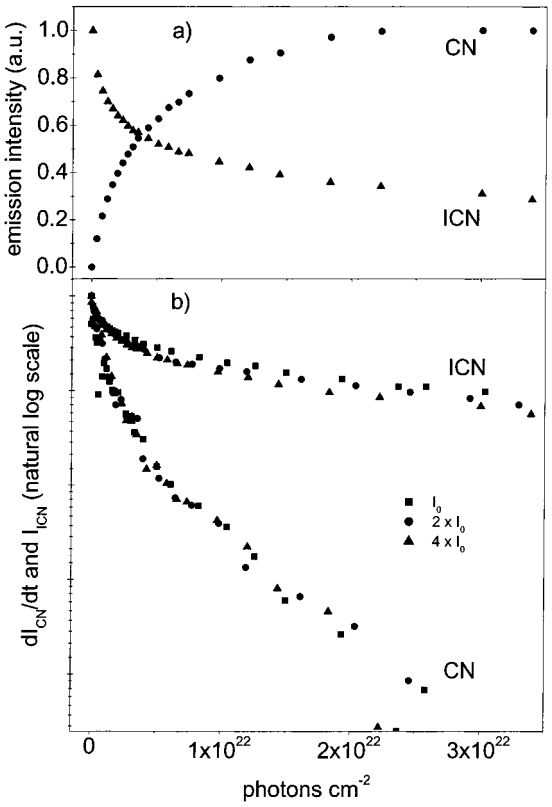

Figure 7. (a) Changes in emission intensity of the broad IR band (Figure 5) at 800 nm and the CN $A^2\Pi \rightarrow X^2\Sigma^+$ (1,0) emission at 900 nm (Figure 6) as a function of irradiation by a focused femtosecond laser at 260 nm and 4 K. (b) Logarithmic plot of the IR emission intensity and the slope of the CN emission growth for different laser intensities ($I_0 \approx 1 \times 10^{10}$ W cm^{-2}). Sample prepared at 20 K, $c \approx$ 1:1000.

of the CN $A^2\Pi \leftarrow X^2\Sigma^+$ (0,4) and (0,3) transitions (instead of UV excitation) yields similar emission bands at 900 nm, and the structures present in the emission spectra after photolysis and before annealing (Figure 6a,b) can clearly be identified as due to special trapping sites of CN by their excitation spectra. These sites also give rise to $A^2\Pi \rightarrow X^2\Sigma^+$ (9,v″) and (8,v″), v″ = 2, 3, ..., 6, emission upon excitation of the $B^2\Sigma^+$ state at 386 nm.[48] Such emission has not been reported for matrix-isolated CN, but a similar spectrum has been observed for CN isolated in Ar clusters with ICN as a precursor.[36] In our matrixes, the intensity of these emissions diminishes strongly in favor of the low-lying A−X transitions (v′,0), v′ = 1, 2, 3, of the main site after annealing. When the $A^2\Pi \rightarrow X^2\Sigma^+$ (1,0) emission at 900 nm is excited via A- or B-state excitation, a lifetime of a few microseconds is measured [with a rise time corresponding to the (2,0) emission lifetime]. On the other hand, a lifetime indistinguishable from that of the broad emission at 800 nm (320 μs) is measured when the sample is excited at 250 nm. In fact, CN does not absorb at this wavelength, but it is excited via reabsorption of the broad near-infrared fluorescence band. We emphasize that excitation of a freshly grown sample at 386 nm ($B^2\Sigma^+ \leftarrow X^2\Sigma^+$ transition of CN) or at a wavelength corresponding to the $A^2\Pi \leftarrow X^2\Sigma^+$ absorption bands of CN does not yield fluorescence. The CN emission (and absorption) bands only form under continued UV irradiation, while the intensity of the broad infrared emission decreases.

2. Photolysis. Figure 7a shows the intensities of the broad IR emission and the CN band at 900 nm as a function of irradiation (the sample was grown at 20 K, and the measurements were carried out at 4 K). This time, the very stable third harmonic of a Ti:sapphire-seeded femtosecond amplifier at 260 nm was used to measure several sets of data under identical conditions and to obtain large irradiation doses (note the different scale with respect to Figure 3). At the same time, the intense femtosecond laser "self-anneals" the irradiated spot on the sample, as (after a few minutes) predominantly one CN site is seen. Very similar data have, however, also been obtained with a different sample under long irradiation using an intense nanosecond laser. Qualitatively, the CN emission grows as the broad IR emission decreases, and the similarity of the fluorescence growth and decay curves for different laser intensities shows that the processes involved are due to single-photon absorption. The time constants for the growth of the CN band and for the decrease in IR emission intensity are, however, similar only for short irradiation times (less than 10^{21} photons cm^{-2}), and the kinetics are clearly nonexponential. This can be seen in Figure 7b, where dI_{CN}/dt and I_{IR} are plotted together on a logarithmic scale (a monoexponential growth of CN at the cost of the species responsible for the IR emission would yield two parallel curves in such a plot). The initial slope that can be fit to the CN data, $\beta = (5 \pm 1) \times 10^{-21}$ cm^2, is compatible with the 3% estimate for the permanent dissociation efficiency obtained from the absorption measurements (slow component in Figure 3b). In comparison, the long-time decay of the IR emission is slower by a factor of ~40, while the rate of CN emission growth is changing less drastically. We recall, however, that the connection between the CN emission and the broad IR band intensity is complicated by the fact that CN radicals are excited by reabsorption of this band, and earlier saturation of the growth of the CN emission is therefore expected. Indeed, the CN emission intensity decreases again, along with the ICN emission, after very long irradiation. In addition, the absorption and scattering properties of the samples change significantly for such large irradiation doses, as witnessed by a steady decrease in the UV laser transmission with time.

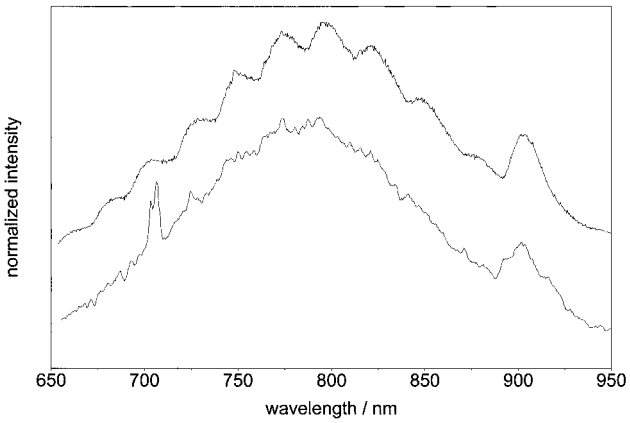

Figure 8. Lower trace: thermoluminescence spectrum recorded during annealing of a previously irradiated sample, with the excitation laser turned off. The spectrum recorded upon laser excitation at 248 nm and 12 K is shown for comparison in the upper trace. The latter signal is orders of magniude stronger, and intensities have been normalized.

Upon subsequent annealing of the sample, the broad emission band recovers part of its intensity, while the CN absorption band at 386 nm loses in strength, as described above. Because a transformation of CN sites with different quantum yields for the $A^2\Pi \rightarrow X^2\Sigma^+$ (1,0) transition takes place during annealing, the changes in CN emission intensity are not directly correlated with those observed in absorption.

During the annealing process, and during the time when the laser is turned off, the broad emission band can be detected as thermofluorescence (Figure 8, lower trace), although it is less

modulated than under laser excitation (upper trace in Figure 8). The weaker modulation is due to phonon-induced processes, as mentioned above. The CN $A^2\Pi \rightarrow X^2\Sigma^+$ (1,0) band at 900 nm is also present in this thermoluminescence spectrum during annealing of the sample, which is a further indication that CN is excited by reabsorption of photons from the broad emission band.

IV. Discussion

Two sets of results have been obtained with regard to the spectroscopy of ICN and its photoproducts in Ar matrixes and the mechanisms of photoproduct formation. The assignment of the spectroscopic features will be discussed first, bearing in mind, however, that the kinetics also help in attributing them.

A. Assignment of the Absorption Spectra. The recording of absorption spectra of fresh samples and the use of very pure solid ICN leave little doubt that the only absorbing molecule in our sample before laser irradiation is ICN. Therefore, the broad absorption band with a maximum at 242 nm in Figure 2a is the so-called $\tilde{A}$ band of ICN. It exhibits a slight blue shift with respect to the gas-phase band (centered at 250 nm),[41] which is probably due to matrix-induced shifts of the absorbing $^1\Pi_1$, $^3\Pi_1$, and $^3\Pi_{0^+}$ states, but which could also indicate a slight relative enhancement in oscillator strength of the $^1\Pi_1 \leftarrow X^1\Sigma_{0^+}$ transition with respect to the $^3\Pi_{0^+} \leftarrow X^1\Sigma_{0^+}$ transition. The rise in absorption below 210 nm in Figure 2a is caused by the so-called α band of ICN, which extends far beyond the cutoff wavelength of our setup and is an order of magnitude stronger than the $\tilde{A}$ band in the gas phase.[40]

Excitation of the $\tilde{A}$ band of ICN causes the rapid formation of a photoproduct with a (slightly shifted and narrower) absorption band in the same region. The kinetics of formation (very fast saturation under 250-nm excitation) of this new UV absorption feature closely resemble the dynamics observed by Haas et al.[37] for the formation of UV irradiation-induced IR bands. These IR bands at 2057 cm^{-1} and 494 cm^{-1} are stable upon annealing (just as the 245-nm absorption band of Figure 2 is) and were attributed to the INC isomer with the help of quantum chemical calculations.[38] A further parallel between the IR and the UV absorption bands is that they disappear under consecutive irradiation in the 380-nm region.[37] In the infrared study, saturation of INC formation was found to occur after a ~3% loss of ICN, and this was tentatively explained by a possible dynamic equilibrium between INC and ICN, each of which can transform into the other only by absorption of a UV photon.[38] To explain the IR kinetic data, a much larger absorption coefficient for INC than for ICN at 250 nm was postulated. This interpretation is now corroborated by our measurements. Indeed, when ICN is excited outside the new INC absorption band in the far UV at 193 nm (presumably in the α band), much more of the product is formed. An ICN $\leftrightarrow$ INC equilibrium is reached much later under 193-nm irradiation and is shifted in favor of INC. Following this interpretation, subsequent irradiation at 250 nm must shift the equilibrium back toward ICN, in agreement with our observation that the new absorption band at 245 nm, formed by 193-nm irradiation, strongly decreases under subsequent 250-nm irradiation. We therefore assign the irradiation-induced absorption band at 245 nm to the INC isomer.

Because ICN is also regenerated by irradiation in the 350−400-nm region (after INC formation under 250- or 193-nm irradiation), we postulate an additional INC absorption band in this wavelength regime, which is responsible for the very small increase in absorption under UV irradiation that we believe can be seen in this wavelength regime (Figure 2c). Because of its weakness, however, its growth kinetics could not be recorded.

Morokuma et al. have calculated the potential surfaces of I−CN for all orientations of the CN fragment. They predict that the linear configurations ICN and INC are the most stable in both the ground- and the excited-state surfaces that make up the $\tilde{A}$ band of ICN.[13] In the ground state, the INC potential minimum lies about 10 000 cm^{-1} above that of ICN, and both minima are separated by a barrier of about 2 eV, which explains why annealing at 30 K does not transform one isomer into the other.

According to the calculated excited-state potential curves, the INC isomer should absorb in the 400−500-nm region (see Figure 1). Given the good agreement of these curves with the experimental absorption spectrum in the ICN configuration, the $^1\Pi_1$, $^3\Pi_{0^+}$, and $^3\Pi_1$ states cannot be responsible for the 245-nm band of INC, and even the weak INC absorption at wavelengths below 400 nm is probably due to transitions to higher excited states of INC. Unfortunately, to our knowledge, no higher excited potential energy surfaces are known for the INC isomer, and an assignment of possible states can only be based on known transitions of ICN. Within these limitations, the most likely candidate for the 245-nm band of INC is the analogue of the α band of ICN, which lies about 17 000 cm^{-1} above the $\tilde{A}$ band.[13]

Assuming an equilibrium ratio between INC and ICN under 250-nm irradiation of 40:1, as inferred from the infrared data of Haas et al.,[38] and knowing from our data that the ICN absorption and the irradiation-induced absorption band at 245 nm are almost equal in strength (with a ratio of ~5:4) at this wavelength, we can estimate the extinction coefficient for the transition responsible for the 245-nm band to be $\epsilon \approx 3000$ L mol^{-1} cm^{-1} (using $\epsilon = 100$ L mol^{-1} cm^{-2} for ICN). Because the new band is slightly narrower, the ratio of oscillator strengths of the ICN $\tilde{A}$ band and the transition responsible for the 245-nm absorption band is then on the order of 1:25.

For comparison, the oscillator strengths measured for the $\tilde{A} \leftarrow X^1\Sigma_{0^+}$ and $\alpha \leftarrow X^1\Sigma_{0^+}$ transitions of gas-phase ICN by Felps et al. are 4.7×10^{-3} and 2.3×10^{-2}, respectively,[40] which yields a ratio of 1:5.

Turning the argument around and assuming a 1:5 ratio for the oscillator strengths of the $\tilde{A}$ band of ICN and the new band (due to INC), our data would indicate a ~10% conversion of ICN into INC at 250 nm.

Finally, we turn to the narrow band at 370 nm, which also grows with UV irradiation. Just as the INC band at 245 nm, it disappears again upon 370−400-nm irradiation, but its growth kinetics under 193-nm irradiation seem to differ from those of the 245-nm band (Figure 4), suggesting a different origin. In addition, its formation is enhanced after annealing of the sample, whereas the 245-nm band formation is unaffected. Finally, its strength with respect to the 245-nm band varies from sample to sample. Nevertheless, the reversibility of the process leading to the formation and disappearance of the 370-nm structure and its presence in all our samples suggest that it belongs to a photoproduct of ICN. Its proximity to the $B^2\Sigma^+ \leftarrow X^2\Sigma^+$ transition of CN at 386 nm may indicate CN, trapped in a specific site. However, the energy shift with respect to the main site of CN is much too large, especially in comparison with the different CN trapping sites identified in our samples under $A^2\Pi \leftarrow X^2\Sigma^+$ excitation (see Figure 6). In addition, just like the INC absorption band, the 370-nm band is stable under annealing, and excitation at 370 nm does not lead to (CN) emission.

A more likely candidate species responsible for the 370-nm absorption band is, therefore, an ICN isomer, possibly in a nonlinear configuration, that is stabilized in a specific trapping site. In fact , Haas et al.[37] reported two IR bands, at 2057 cm^{-1} (attributed to INC) and at 2059 cm^{-1}, that form upon UV-irradiation of ICN-doped Ar, and they clearly established that both stem from monomers. As in our case, the relative intensity of the two bands varied from sample to sample in the IR experiments. We therefore tentatively assign the 370-nm absorption band to INC, and attribute the difference in kinetics with respect to the broad absorption band at 245 nm to the presence of two different trapping sites, possibly with different relative transition probabilities at 245 and 370 nm.

The possibility can also not be excluded that the different behavior of the 370- and 245-nm absorption bands arises from the interaction of some molecules with nearby ICN neighbors, even though our data provide no evidence for a systematic dependence of the 370-nm/245-nm absorption intensity ratio on concentration.

B. Assignment of the Emission Spectra. There are a number of arguments suggesting that the IR progression in the 800-nm region (Figure 5) is due to emission of ICN molecules: (a) The emission is immediately present after growth of the sample and does not grow on a time scale observed for the formation of photoproducts (INC and CN). (b) It decays under UV irradiation, and this decay is accompanied by the growth of the CN emission. Both follow the same kinetics at early times. (c) After UV irradiation of the samples, the emission is observed as thermofluorescence upon annealing. This is accompanied by a decrease in CN absorption. The thermofluorescence is due to recombining I and CN fragments, with ICN as the most probable outcome.

These arguments alone, however, do not exclude the possibility that, after excitation of ICN, the IR fluorescence may be due to subsequent recombination in the INC configuration. This possibility must be considered seriously, because our absorption data suggest a continuous photoinduced transformation of ICN into INC. In this case, however, the ICN fluorescence should decrease in intensity until an ICN−INC equilibrium is reached. Under 250-nm irradiation, such a decrease may escape detection because of the rapidly established equilibrium and the very small conversion of ICN into INC (~3% according to the IR data[37]), but even under 193-nm excitation, where the 800-nm fluorescence is also seen and much more ICN is converted into INC, a change in fluorescence intensity has only been observed on the (much longer) time scale of CN fragment formation.

We therefore conclude that the broad, weakly structured IR fluorescence observed upon excitation of the $\tilde{A}$ (and α) bands of ICN accompanies the relaxation of this molecule in the original configuration.

Previous studies by Bondybey and co-workers on alkyl iodides trapped in rare-gas matrixes[44] have shown evidence for fluorescence from recombination of matrix-caged fragments following the excitation of purely repulsive excited states. These quasi-bound states have their potential minima at internuclear distances significantly longer than those of the molecule in the ground state. They give rise to long progressions, having spacings characteristic of high-lying vibrational levels of the ground state. We believe that a situation similar to that of the alkyl halides is encountered upon UV excitation of ICN in solid argon.

Indeed, three vibrational modes in the ground state have been identified for ICN in Ar,[38] which are the I−C stretch at 487 cm^{-1}, the C−N stretch at 2171 cm^{-1}, and the bending mode at 317 cm^{-1}. For comparison, the corresponding values for INC are 494 cm^{-1} (I−N stretch) and 2057 cm^{-1}(CN-stretch). The vibrational spacing of 415 cm^{-1} that we observe for the IR fluorescence of ICN is thus typical for high vibrational levels of the I−CN stretch mode, which is the dominant reaction coordinate for photodissociation and recombination. Fitting our data to the energy levels of a one-dimensional Morse potential[13] of ICN in the ground state, we find that the peak of emission at 11 800 cm^{-1} corresponds to the $v'' = 19 \pm 1$ vibrational level of the I−C stretch. This level is situated about 16 800 cm^{-1} below the $I(^2P_{3/2}) + CN(^2\Sigma^+)$ dissociation limit. Also according to this fit, the minimum of the emitting state is located at an I−CN distance of 3.18 Å, 5000 cm^{-1} below the first dissociation limit. A similar fit, using the ground-state potential in the INC configuration,[13] yields $v'' = 13$ for the vibrational level (I−N stretch), attained by the emission at 11 800 cm^{-1}, and a minimum of the excited state at $R = 3.0$ Å (I−CN distance). This excited-state minimum would be located about 2000 cm^{-1} above the $I(^2P_{3/2}) + NC(^2\Sigma^+)$ dissociation limit, a region where no electronic states are located according to the ab initio calculations (see Figure 1). This provides a further argument in favor of ICN rather than INC as being responsible for the observed IR emission. We believe that such a one-dimensional approach to assigning the IR emission is justified because the emission is evidently due to a completely relaxed excited-state population and because the minima of all possible excited states correspond to the linear configurations of ICN or INC.[13] We do realize, however, that the ground-state potential surface of ICN may deviate considerably from the Morse approximation, especially at large internuclear distances. Nevertheless the above considerations limit the choice of emitting states to the $^3\Pi_1$ or $^3\Pi_2$ states of ICN, which correlate with the $I(^2P_{3/2}) + CN(^2\Sigma^+)$ asymptote. According to ab initio calculations, both have shallow minima of 900 cm^{-2} and 2500 cm^{-2}, respectively, at an I−CN distance near 3.4 Å.[12,13] The $^3\Pi_1$ state is responsible for the red wing in the $\tilde{A}$ band absorption spectrum of ICN near 280 nm with an oscillator strength of $f = 0.46 \times 10^{-3}$ for the $^3\Pi_1 \leftarrow X^1\Sigma_{0^+}$ transition in the Franck−Condon region.[13] The use of this value in connection with the emission at 800 nm yields an estimate for the radiative lifetime of the $^3\Pi_1$ state of ~20 μs. Only an unrealistically strong decrease in the $^3\Pi_1 \rightarrow X^1\Sigma_{0^+}$ transition moment with I−CN distance could reconcile this estimated lifetime for $^3\Pi_1$ with the measured value of 320 μs. Also note that, in neon matrixes, a 650-μs lifetime is found for the same transition.[45]

The $^3\Pi_2$ state, on the other hand, is the lowest-lying excited state of ICN. It is not observed in absorption because the $^3\Pi_2 \leftarrow X^1\Sigma_{0^+}$ transition is strongly forbidden in the gas phase. In matrixes, however, this transition can become weakly allowed, and emission from this state may be observed, especially in the absence of efficient nonradiative relaxation paths. Energy considerations also favor the lowest-lying $^3\Pi_2$ state as the state responsible for the IR emission. Given these arguments, we therefore assign the weakly structured emission band shown in Figure 5 to the $^3\Pi_2 \leftarrow X^1\Sigma_{0^+}$ transition.

To summarize, after excitation of ICN to the dissociative $\tilde{A}$ continuum, the fragments recombine because of caging by the surrounding Ar matrix. Part of the excited-state population gets trapped in the minimum of the $^3\Pi_2$ excited state in the linear ICN configuration. This state decays radiatively with a lifetime of 320 μs, leading to the IR emission shown in Figure 5. Because this emission is also observed as thermofluorescence, the same excited state is also attained by thermally recombining I and

CN fragments. A more detailed discussion of the ICN emission, including data from other matrixes and a comparison with MD calculations, is presented elsewhere.[45]

C. Photoinduced Dynamics. The above results and assignments lead to a complex picture of the photochemistry of ICN under UV irradiation, which includes isomerization, dissociation, and recombination. These different processes will now be discussed separately.

1. Isomerization. The behavior of ICN in liquid and solid argon during the first few picoseconds after Ã-band excitation has been the subject of several molecular dynamics simulations, using the potential surfaces calculated by Morokuma and coworkers in connection with the relevant fragment−rare gas interactions derived from atom−atom potentials.[27,29,30] The most extensive calculations were carried out by Fernandez-Alberti et al.,[30] as they considered all potential surfaces involved in the dissociation−recombination process, namely, the ground state, the $^3\Pi_{0^+}$ state, and the two components of the $^1\Pi_1$ and $^3\Pi_1$ surfaces, with the exception of the $^3\Pi_2$ and $^3\Pi_{0^-}$ states, which carry no oscillator strength and for which no potential surface is available. In addition, they carried out a full treatment of the matrix-induced nonadiabatic couplings occurring in the region of the asymptotic limit, using the diatomic-in-molecules (DIM) treatment combined with molecular dynamics with quantum transitions (MDQT). In solid Ar, these simulations predict a large yield for recombination of the fragments as INC on the excited-state surfaces after collision of the CN fragment with the closed-shell rare gas atoms. According to the trajectories of ref 30, ICN quickly switches from the originally excited $^3\Pi_{0^+}$ state into the $^1\Pi_1$ state, where predominantly excited molecules in the INC configuration are produced. After 3 ps, already 70% of the molecules occupy hot vibrational levels in the ground state (INC configuration). The subsequent much slower vibrational relaxation on the ground-state surface is, however, more difficult to treat in simulations. In fact, during the final relaxation process, many molecules may flip back to the ICN configuration, which is more stable by $\sim$10 000 cm^{-1} than the isomer. This process is being simulated at present.[46]

As mentioned before, the most convincing experimental evidence for the formation of INC was provided by Haas and co-workers.[37,38] To explain the observed saturation of ICN → INC conversion after a 2.6% decrease in ICN concentration as suggested by their IR absorption data, they postulated a strong UV absorption of INC, which can revert back to ICN upon absorption of a UV photon. In assigning the irradiation-induced UV absorption band at 245 nm to the INC species, we confirm this interpretation, and we are able to draw a more detailed picture of the ICN ↔ INC isomerization process. Upon 250-nm irradiation, the absorption band assigned to INC grows to almost the same strength as the original ICN absorption. Thus, the probability of exciting an ICN or INC molecule at 250 nm is almost equal once equilibrium is reached, independent of the relative number of the two species. As a consequence, the probability of forming INC from excited ICN must be similar to the probability of forming ICN from excited INC.

The quantum efficiency for isomerization can be estimated under the assumption of a back rate k(INC→ICN) 40 times larger than the isomerization rate k(ICN→INC), as required for equilibrium after a 2.6% conversion of ICN to INC. Simulated growth curves for quantum efficiencies of 30% and 70% are compared to the experimental INC growth data in the inset of Figure 3. Within the experimental error, and especially keeping in mind the estimated uncertainty of a factor 2 for the photon flux, the probability of isomerization is bound by these values, in qualitative agreement with MD simulations.[30]

The similar likelihood of the ICN* → INC and INC* → ICN processes further suggests that the INC−ICN branching after excitation could be largely independent of the initial configuration of the molecule. In fact, because of the very similar masses of the CN fragment and Ar, most of the kinetic energy induced in the molecule upon excitation is very efficiently transferred to the matrix during the first collisions with the closed-shell rare gas atoms, as confirmed by MD simulations.[30] In the absence of kinetic energy, the subsequent relaxation process will then be dominated by the topology of the potential surfaces involved.

Indeed, the $^3\Pi_2$ state in the ICN configuration, which gives rise to the broad fluorescence band discussed above, is equally attained upon excitation of INC and ICN at 250 nm. This can be deduced from the observation that initial preparation of a large number of INC molecules by 193-nm irradiation leads to a temporary strong increase in the ICN fluorescence intensity under subsequent 250-nm excitation, until the 250-nm equilibrium is reestablished and the INC absorption band is reduced. At the same time, the presence of the IR emission upon 193-nm excitation of ICN suggests that relaxation on the Ã band potential surfaces is an important bypass to the ICN → INC conversion under α-band excitation. Under 193-nm irradiation, the 245-nm band grows $\sim$4 times stronger than the original ICN absorption band and, therefore, $\sim$5 times stronger than under 250-nm irradiation. Assuming a 3% conversion of ICN into INC under 250-nm irradiation, this means that 15% of ICN is transformed into INC at 193 nm before equilibrium is reached. Indeed, the presence of ICN fluorescence after saturation of the absorption band growth shows that ICN does not disappear completely even under α-band irradiation. On the other hand, ICN does not absorb in the 400-nm region, where INC does show a transition, and all INC can be converted back into ICN under irradiation in this wavelength regime. The relative concentrations of ICN and INC in Ar matrixes can therefore be easily controlled by the choice of irradiation wavelength. We believe that the determining factor in establishing the equilibrium is the relative absorption coefficient at a given photon energy rather than the dependence of the quantum yield of isomerization on the initially accessed excited state.

On a more general perspective, we have here a typical example of how the outcome of a chemical reaction, the isomerization of ICN, can be controlled by environment effects (which exert the necessary steric hindrance) and the appropriate choice of radiation energy.

2. Cage Exit of Fragments and Permanent Dissociation. Our results clearly establish the occurrence of permanent dissociation of ICN in solid Ar, leading to the stabilization of I and CN fragments. The quantum efficiency for dissociation is, however, strongly dependent on sample preparation conditions and the sample temperature during irradiation. In poor-crystalline-quality, strongly scattering samples, grown at 4 K, we observe very efficient dissociation, which is probably favored by an irregular crystal structure surrounding a substantial number of ICN impurities. Early ESR studies by Easley and Weltner,[33] which clearly identified the production of CN from irradiated ICN in Ar, were conducted on such low-temperature condensates. Slow growth of ICN-doped Ar solids at 20 K, on the other hand, yields samples of high optical quality. With such samples, comparable to those grown by Haas et al.,[37] we measure a dominant CN growth rate at 12 K that corresponds to an ICN dissociation efficiency of approximately 3%, more

than 1 order of magnitude smaller than that found for samples grown at 4K.

The initially faster increase in CN absorption in our "high-quality" samples (efficiency > 30%, Figure 3b) is most likely due to imperfect ICN trapping sites, reminiscent of those present in samples of poor crystalline quality. We tentatively attribute the coincidence of INC saturation and the vanishing of the fastest CN growth component after an irradiation dose of $\sim 2 \times 10^{18}$ photons cm^{-2} to the fact that, at this point, almost all ICN molecules have undergone at least one ICN $\leftrightarrow$ INC conversion cycle. During this cycle, a large amount of energy (2×5 eV) is transferred to the Ar atoms around each molecule, which may lead to an elimination of unstable ICN trapping sites. Note that the increase in absorption at the irradiation wavelength due to INC formation and a subsequent decrease in effective photon flux are much too small to account for the observed drastic change in the CN growth rate. The possibility can also be excluded that INC serves as an intermediate for the formation of CN fragments, as in this case, the rate of CN formation should rapidly increase (and not decrease) until the ICN/INC equilibrium is established.

In high-quality samples, only a small number of CN fragments are produced in the initial fast process. In addition, the CN site emitting at 915 nm that is predominantly formed in low-quality samples (Figure 6a) is absent. The dominant ICN dissociation process in carefully prepared matrixes (3% efficiency at 12 K, Figure 3) is thus not due to remaining "imperfect" environments. More importantly, the ICN fluorescence continues to decrease even after a 60% loss in intensity under 260-nm irradiation (Figure 7), and it is very unlikely that exclusively those ICN sites that favor dissociation should also show radiative recombination. The observed stabilization of CN fragments must therefore occur with the regular embedding of ICN in Ar matrixes.

The fact that CN formation was not observed by Haas and co-workers can be due to a combination of circumstances: (a) The CN 0−1 vibrational absorption in solid Ar at 2044 cm^{-1} is orders of magnitude weaker than the visible electronic $X^2\Sigma^+ \leftarrow B^2\Sigma^+$ absorption,[49] and the presence of a weak population of CN is, therefore, much more difficult to detect by IR spectroscopy. (b) The sources for UV irradiation employed in that study were much weaker than our excimer laser or YAG-pumped parametric oscillator. (c) At the more elevated temperatures of the IR study, the recombination rate of I and CN fragments is high.

Indeed, the near-unity CN-to-Ar mass ratio leads to a very efficient kinetic energy transfer upon CN−Ar collision, and it is clear that, in the event of dissociation, the CN fragment will stabilize in a site that lies in the vicinity of the corresponding I atom (the original ICN site). This is confirmed by our observation of red-shifted A−X emission bands from CN radicals that are occupying sites different from those usually found for matrix-isolated CN. The vicinity of I and CN after cage exit also favors thermally induced recombination, as evidenced by the loss of CN absorption upon annealing. During this recombination process, all electronic states correlating to the $I(^2P_{3/2}) + CN(X^2\Sigma^+)$ asymptote can, in principle, be accessed. In particular, we observe recombination and trapping on the $^3\Pi_2$ surface that subsequently gives rise to thermofluorescence. The recombination rate of previously stabilized fragments increases with temperature. We thus observe a much slower growth of the CN fragment absorption when the sample is held at 20 K instead of 12 K during irradiation.

A dissociation mechanism involving thermally induced recombination of the type

$$\mathrm{ICN} \rightleftharpoons \mathrm{I}\cdots\mathrm{CN} \rightarrow \mathrm{I} + \mathrm{CN} \qquad (2)$$

may also explain the leveling off of the ICN emission decay observed in Figure 7. In such a scenario, the ICN $\rightarrow$ I···CN fragment separation would dominate the kinetics at early times, until equilibrium with thermally induced ICN $\leftarrow$ I···CN recombination leads to an effectively stable ICN population. The much slower stabilization process I···CN $\rightarrow$ I + CN, which produces CN in its usually observed site, would be responsible for the very slow decrease in ICN emission at long times. A quantitative analysis of the emission data along this line is under way but faces the difficulty of secondary effects such as changes in scattering and the reabsorption of ICN emission by CN fragments.

To summarize, the measured probability for photodissociating ICN embedded in an Ar matrix is dependent on the temperature during irradiation, whereas the "actual" quantum yield strongly depends on the sample growth conditions, especially the growth temperature, i.e., the local structure. The dependence of the cage exit probability on the structure of the environment is also borne out by the classical MD simulations. In liquid Ar, Amatatsu and Morokuma[27] and Krylov and Gerber[29] reported a ~40% probability for permanent dissociation. In solid Ar, with a perfect fcc lattice around the ICN molecule in a bi-substitutional site, Krylov and Gerber[29] and Fernandez-Alberti et al.[30] report a zero probability for cage exit.

The absence of cage exit in the MD calculations, while certainly a good reason for the low yield observed in our experiments, may be due to the fact that they were carried out at a classical temperature of 4 K, which does not take into account the quantum mechanical zero-point motion at this temperature. It is not unlikely that the sampling of a larger set of initial configurations (for example, by artificially raising the temperature in classical trajectory calculations) could lead to trajectories that demonstrate CN cage exit. Fernandez-Alberti et al. have repeated their calculations more recently,[47] using wave-packet dynamics to treat the motion on the ICN coordinates and found a 2% probability for CN cage exit, although they still treated the lattice classically. This value compares very well with our estimate of a 3% quantum efficiency for permanent dissociation.

V. Conclusion

It was shown that excitation of the Ã-band excited-state manifold of ICN embedded in Ar matrixes leads to efficient caging of the CN fragment, radiative recombination as ICN, and formation of the INC isomer.

An absorption band of INC at 245 nm was reported, extending from 220 to 280 nm, and its extinction coefficient was estimated to be 3000 L mol^{-1} cm^{-1}, by making use of previous IR absorption data.[38] Excitation of this band near 250 nm leads to the re-formation of ICN with a probability similar to that of forming INC from ICN at the same wavelength, giving rise to a photostable equilibrium between the two isomers. By excitation of ICN at 193 nm, outside this INC absorption band, five times more ICN molecules can be converted into INC.

The occurrence of permanent dissociation of ICN has been confirmed, and the quantum efficiency was estimated to be 3%, but this value is much larger in matrixes of lesser quality that are grown at lower temperatures. In addition, thermally induced recombination of fragments at temperatures above 10−15 K was shown to lower the apparent rate of dissociation of ICN.

These findings and the varying sensitivity of the different experimental methods employed suffice to explain conflicting views in the literature on the photolysis of ICN in solid argon.

Acknowledgment. We thank the group of Prof. C. Floriani (UNIL) for providing highly purified ICN and S. Fernandez-Alberti, J. Echave, and A. Beswick for communicating results prior to publication. This work was supported by the Swiss National Science Foundation (FNRS) under Grants 2000-050427-97, 2160-050330-97, and 2000-053811-98.

References and Notes

(1) Chergui M.; Schwentner, N. *Trends Chem. Phys.* **1992**, *2*, 89.
(2) Apkarian, V. A.; Schwentner, N. *Chem. Rev.* **1999**, *99*, 1481.
(3) Liu, Q.; Wan, C.; Zewail, A. H. *J. Phys. Chem.* **1996**, *100*, 18666.
(4) Schriever, R.; Chergui, M.; Ünal, Ö; Schwentner, N.; Stepanenko, V. *J. Chem. Phys.* **1990**, *93*, 3245.
(5) Schwentner, N.; Chergui, M.; Kunz, H.; McCaffrey, J. G. *Reaction Dynamics in Clusters and Condensed Phases*; Kluwer Academic Publishers: Amsterdam, 1994; pp 521−537.
(6) Gödderz, K.-H.; Schwentner, N.; Chergui, M. *Chem. Phys.* **1996**, *209*, 91.
(7) McCaffrey, J. G.; Kunz, H.; Schwentner, N. *J. Chem. Phys.* **1992**, *96*, 155.
(8) Zoval, J.; Apkarian, V. A. *J. Phys. Chem.* **1994**, *98*, 7945.
(9) Zadoyan, R.; Almy, J.; Apkarian, V. A. *Faraday Discuss.* **1997**, *108*, 255.
(10) Zadoyan, R.; Li, Z.; Martens, C. C.; Apkarian, V. A. *J. Chem. Phys.* **1994**, *101*, 6648.
(11) Liu, Q.; Wang, J.-K.; Zewail, A. H. *Nature* **1993**, *364*, 427.
(12) Yabushita, S.; Morokuma, K. *Chem. Phys. Lett.* **1990**, *175*, 518.
(13) Amamtatsu, Y.; Yabushita, S.; Morokuma, K. *J. Chem. Phys.* **1994**, *100*, 4894.
(14) Qian, J.; Tannor, D. J.; Amatatsu, Y.; Morokuma, K. *J. Chem. Phys.* **1994**, *101*, 9597.
(15) Wang, Y.; Quian, C. X. W. *J. Chem. Phys.* **1994**, *100*, 2707.
(16) Wei, H.; Carrington, Jr. T. *J. Chem. Phys.* **1996**, *105*, 141.
(17) Pitts, W. M.; Baronavski, A. P. *Chem. Phys. Lett.* **1980**, *71*, 395.
(18) Goldfield, E. M.; Houston, P. L.; Ezra, G. S. *J. Chem. Phys.* **1986**, *84*, 3120.
(19) Nadler, I.; Mahgerefteh, D.; Reisler, H.; Wittig, C. *J. Chem. Phys.* **1985**, *82*, 3885.
(20) Black, J. F.; Waldeck, J. R.; Zare, R. N. *J. Chem. Phys.* **1990**, *92*, 3519.
(21) Black, J. F. *J. Chem. Phys.* **1993**, *98*, 6853.
(22) Hasselbrink, E.; Waldeck, J. R.; Zare, R. N. *Chem. Phys.* **1988**, *126*, 191.
(23) Black, J. F.; Hasselbrink, E.; Waldeck, J. R.; Zare, R. N. *Mol. Phys.* **1990**, *71*, 1143.
(24) Rosker, M. J.; Dantus, M.; Zewail, A. H. *Science* **1988**, *241*, 1200.
(25) Dantus, M.; Rosker, M. J.; Zewail, A. H. *J. Chem. Phys.* **1988**, *89*, 6128.
(26) Benjamin, I.; Wilson, K. R. *J. Chem. Phys.* **1989**, *90*, 4176.
(27) Amatatsu, Y.; Morokuma, K. *Chem. Phys. Lett.* **1995**, *245*, 469.
(28) Benjamin, I. *J. Chem. Phys.* **1995**, *103*, 2459.
(29) Krylov, A. I.; Gerber, R. B. *J. Chem. Phys.* **1994**, *100*, 4242.
(30) Fernandez-Alberti, S.; Halberstadt, N.; Beswick, J. A.; Echave, J. *J. Chem. Phys.* **1998**, *109*, 2844.
(31) Raftery, D.; Gooding, E.; Romanovsky, A.; Hochstrasser, R. M. *J. Chem. Phys.* **1994**, *101*, 8572.
(32) Wan, C.; Gupta, M.; Zewail, A. H. *Chem. Phys. Lett.* **1996**, *256*, 279.
(33) Easley, W.; Weltner, W., Jr. *J. Chem. Phys.* **1970**, *52*, 197.
(34) Carr, B. R.; Chadwick, B. M.; Cobbold, D. G.; Grzybowski, J. M.; Long, D. A.; Marcus-Hanks, D. A. M. *Ber. Bunsen-Ges. Phys. Chem.* **1978**, *82*, 98.
(35) Leutwyler, S.; Maier, J. P.; Spittel, U. *J. Chem. Phys.* **1985**, *83*, 506.
(36) Lin, H.-S.; Erickson, M. G.; Lin, Y.; Basinger, W. H.; Lawrence, W. G.; Heaven, M. C. *Chem. Phys.* **1994**, *189*, 235.
(37) Fraenkel, R.; Haas, Y. *Chem. Phys. Lett.* **1993**, *214*, 234.
(38) Samuni, U.; Kahana, S.; Fraenkel, R.; Haas, Y.; Danovich, D.; Shaik, S. *Chem. Phys. Lett.* **1994**, *225*, 391.
(39) Milligan, D. E.; Jacox, M. E. *J. Chem. Phys.* **1967**, *47*, 278.
(40) Felps, W. S.; Rupnik, K.; McGlynn, S. P. *J. Phys. Chem.* **1991**, *95*, 639.
(41) Hess, W. P.; Leone, S. R. *J. Chem. Phys.* **1987**, *86*, 3773.
(42) Helbing, J.; Chergui, M., to be published.
(43) Wurfel, B. E.; Schallmoser, G.; Lask, G. M.; Agreiter, J.; Thoma, A.; Schlachta, R.; Bondybey, V. E. *Chem. Phys.* **1993**, *174*, 255.
(44) Brus, L. E.; Bondybey, V. E. *J. Chem. Phys.* **1976**, *65*, 71.
(45) Helbing, J.; Chergui, M.; Fernandez-Alberti, S.; Echave, J.; Halberstadt, N.; Beswick, J. A. *PCCP* **2000**, in press.
(46) Fernandez-Alberti, S.; Echave, J.; Halberstadt, N.; Beswick, J. A., Université Paul Sabatier, Toulouse, France. Private communication, 2000.
(47) Fernandez-Alberti, S.; Echave, J.; Engel, V.; Halberstadt, N.; Beswick, J. A. *J. Chem. Phys.* **2000**, *113*, 1027.
(48) Note that significant site effects are only detected in A−X transitions and that the B state absorption band at 386 nm is due to the sum of all sites. This could be due to the fact that the X and B states of CN are of the same symmetry ($^2\Sigma^+$) and almost parallel, whereas the A state is a $^2\Pi$ state, interacting more strongly with the matrix.
(49) Note that, in Easley and Weltner's study,[33] CN was identified by UV absorption but could not be seen in the IR spectra.